31st Annual International Conference of the IEEE EMBS
Minneapolis, Minnesota, USA, September 2-6, 2009

Ultrasonic Viscoelasticity Imaging of Nonpalpable Breast Lesions

Yupeng Qiu, and Michael F. Insana

Abstract — **The prognosis of breast cancer patients improves with early and accurate diagnosis. A small clinical study was conducted with 21 women having a single nonpalpable breast lesion, each detected mammographically with later pathology confirmation. Elasticity images were acquired on each patient to test for the ability to differentiating malignant and benign lesions. The mechanical relaxation time T_1 images showed a tissue-specific T_1 contrast that is negative for all 11 malignant lesions and positive for all 10 benign lesions. Strain images were estimated using a regularized multi-scale optical flow (ROF) algorithm. Adjustments to the input parameters to the ROF and their subsequent effects on T_1 estimation and computation time are shown to have a strong effect of diagnostic performance.**

I. Introduction

Breast cancer is a leading cause of cancer death in woman [1]. A key factor in mortality prevention is early detection and diagnosis of suspicious masses. The first step to the clinical diagnosis of breast cancer is the detection of the breast tumor. This is usually done via manual palpation, and followed up with anatomical imaging and finally, biopsy. Although biopsy is the gold standard for diagnosis, the procedure is invasive, expensive and carries some risk. Noninvasive diagnostic imaging methods are therefore being developed to increase specificity and reduce the number of unnecessary biopsies performed on women each year.

During tumor development, inflammation is commonly observed in early stages. The extracellular matrix (ECM) of local breast stroma is altered by the cancerous growth [2], which often leads to a change in the elastic properties of the tissue. Elasticity imaging is a means for describing the spatial distribution of viscoelastic tissue properties [3], and is used primarily for diagnosis rather than detection.

Several groups have applied elasticity imaging to the diagnosis of focal breast lesions. The consensus is that the relative size of palpable lesions in strain images compared with that in spatially-registered sonograms was a sensitive diagnostic feature [4-6]. Palpable malignant lesions often have some degree of desmoplasia that makes them appear larger on strain images than sonograms. This feature is much less reliable for early stage malignant lesions that are nonpalpable.

We employ a quasi-static [7] ultrasonic method for the viscoelastic breast imaging of a small group of patients. Echo movements are tracked by a broadband ultrasonic probe as it is gently pressed into the skin surface. Step-force amplitudes of 3-6 N are applied suddenly and handheld constant for about 10-20 s while a sequence of radiofrequency (RF) echo frames are recorded to track the slow movement of tissue under a load. The patterns of time-varying strain suggest that breast tissues exhibit viscous creep similar to hydropolymers. A regularized optical flow (ROF) algorithm is applied to the RF echo frames to estimate the time sequence of strain images. Viscoelastic (VE) properties are found by analyzing the time-varying strain at each pixel, fitting it to a Kelvin-Voigt constitutive model to estimate viscoelastic parameters. Performance of the ROF strain algorithm for the purpose of estimating VE tissue parameters was evaluated for different image formation variables. Those leading to maximum diagnostic performance are described.

TABLE I
Breast Lesion Profiles

Disease Type	Diagnosis	Tumor Grades
Benign (10)	Fibroadenoma (7) Fibrocystic Change (2) Dense Collagenous Stroma (1)	N/A
Malignant *(11)*	Infiltrating Ductal Carcinoma (8) Invasive Lobular Carcinoma (2) B-cell lymphoma (1)	Grade 1 (4) Grade 2 (4) Grade 3 (1) Not scored (2)

II. Material and Methods

A. Patient Selection

Patients were randomly selected through the breast clinic at UC Davis Medical Center in Sacramento CA. Permissions were obtained through an approved IRB protocol from 26 patients with a single, nonpalpable lesion identified by mammography prior to core-needle biopsy. Patient ages ranged from 28 to 72 years, and tumor diameter ranged from 0.5 to 2.5 cm. All lesions were potentially malignant and required further tissue analysis. The data from five patients were excluded due to poor acquisition that prevented processing. Biopsy-confirmed diagnoses are summarized in Table I. Details are given in [8].

B. Patient Imaging Techniques

Viscoelastic imaging techniques for breast tissue have

Manuscript received April 23, 2009. This work was supported by the NCI under award No. CA082497 and by the Beckman Institute for Advanced Science and Technology at the University of Illinois.

Y. Qiu is with the Department of Bioengineering and Beckman Institute for Advanced Science and Technology, University of Illinois at Urbana-Champaign, Urbana IL 61801, USA (phone: 217-819-9278; fax: 217-265-0246; e-mail: yqiu2@illinois.edu).

M. F. Insana is with the Department of Bioengineering and Beckman Institute for Advanced Science and Technology, University of Illinois at Urbana-Champaign, Urbana IL 61801 USA (e-mail: mfi@illinois.edu).

been described previously [8]. A Siemens Sonoline Antares ultrasound scanner was used with a VF10-5 linear array transducer operating at 8 MHz to record RF echo data. Patients were positioned supine and breasts were scanned anterior-posterior with the chest wall as compression support. Patients were instructed to hold their breath during the 12-15 s acquisition to minimize breast motion. The RF acquisition frame rate was 17 fps. A downward compressive force of approximately 4 N was manually applied in 1 s via the transducer surface by the sonographer. Sridhar [7] showed that with force sensor, sonographers with limited training were able to keep the force constant within ±0.24 N.

C. ROF Strain Algorithm Parameters

Each strain image is formed from the comparison of two RF echo frames. Therefore, a total of K frames would produce a time series of K-1 strain images. The regularized optical flow algorithm [10] estimates the displacement fields between adjacent frames recorded during compression, and the derivative of the sum displacement field is used to find the strain image. The general equation can be written as [10]

$$\hat{d} = \arg\min_{d\in\Omega}\left(E_1(d) + \alpha E_2(d)\right). \tag{1}$$

Equation (1) minimizes the energy of the cost function to estimate displacement $\hat{d}$. The cost function is constrained by two components: conservation (E_1) and regularization (αE_2), where α is a positive regularization coefficient. E_1 assumes that the echo amplitude is conserved during deformation (minimal decorrelation). The regularization term stablizes the solution by minimizing local displacement variations [10]. Displacement estimates are found by minimizing the total energy, with coefficient α weighting the relative contributions of E_1 and E_2.

There are three key parameters that must be adjusted to apply the ROF strain algorithm to clinical data: α, the search window size, and the numbers of spatial scales over which RF echo data are compared.

ROF employs a multi-scale approach to displacement estimation optimize the convergence of solutions while avoiding local minima. At each scale level $0 \le i \le I$, the image grid is partitioned into N_i equal sized blocks [12] where N stands for the number of blocks, and equation (1) is estimated. The highest scale level (coarsest) estimation is not constrained by the regularization term, thus allowing an initial global minimum to be found. At the lowest scale level (finest), the block size is 4x1 pixels, which corresponds to the ratio of axial and lateral block dimensions [12]. The number of iterations required for the solution to converge increases dramatically as the scale becomes finer. By changing the number of scale levels, both the computation and convergence time will be affected [10].

The search window size depends on the percent tissue compression that occurs between adjacent RF frames recordings. A search window that is too small may render the algorithm unable to find the global energy minimum. A search window that is too big may increase computation time as well as noise, which adds to the estimation uncertainty.

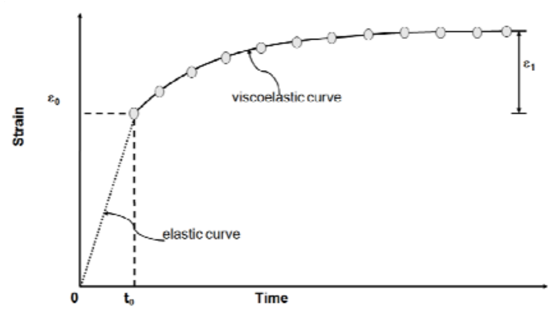

Fig. 1. Typical viscous creep curve and corresponding viscoelastic (VE) parameters for glandular breast tissue. ε_0 describes the instantaneous elastic strain. ε_1 describes the viscoelastic strain amplitude. Compression is applied from time t = 0 until t_0 during which the instantaneous elastic strain is measured. The viscoelastic curve lasts 12 to 15 seconds.

These three parameters were varied to check for the differences in the visual appearance of the strain images, the computation time, and the resultant T_1 estimates. α is varied while the number of scale levels remained at 6 (I = 5) and the search window size remained at 8×2 pixels. The number of scale levels is then varied while α remained at 40 and the search window size remained at 8×2 pixels. Finally, the search window size is varied while α remained at 40 and the number of scale levels remained at 6.

D. Curve Fitting

A time series of strain images are formed as described in Section II (C) using standard multicompression acquisition [9] and the ROF strain imaging algorithm [10]. The creep curve is generated for each strain image pixel (or small group) by plotting strain over time. The VE phase of the curve begins immediately after the initial compression of tissue. VE parameters are extracted from the curves by least-squares fitting of the data to a rheological model. A first order Kelvin-Voigt model [7, 11] is used because our acquisitions were no longer than 15 s and thus did not engage the long-duration VE response:

$$\varepsilon(t) = \varepsilon_0 + \varepsilon_1\left(1 - \exp(-t/T_1)\right). \tag{2}$$

ϵ_0 is the instantaneous elastic strain amplitude occurring immediately after compression (Fig. 1), ϵ_1 is the viscoelastic strain amplitude, and T_1 is the retardation time characterizing the delay in the maximum strain response. Strain delays in stroma are from frictional resistance due to movement of the ECM in viscous interstitial fluids [7]. The three aforementioned VE parameters are estimated for the entire acquired image area, and we obtain a set of four images (B-mode, ϵ_0, ϵ_1 and T_1) for every patient data collected.

E. Parametric Contrast

Small pixel areas of 10×30 or 10×15 were selected in one location within the lesion and another location in the background of each patient image. Average B-mode, ϵ_0, ϵ_1 and T_1 values are estimated from these regions.

The goal of VE imaging is to provide tissue-specific

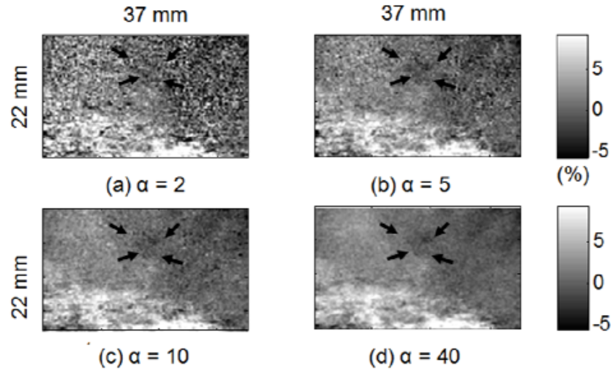

Fig. 2. The lesion region is indicated with black arrows in (a) Strain image ε_0 when regularization coefficient α.= 2. Not enough noise suppression. (b) Strain image when α.= 5. There is some noise suppression. (c) Strain image when α.= 10. Minute noises still exist. (d) Strain image when α.= 40. The image is smooth.

contrast that maximizes diagnostic performance relative to biopsy findings. Lesion contrast is calculated using

$$C = \frac{X_{lesion} - X_{background}}{\left(X_{lesion} + X_{background}\right)/2} = \frac{Difference}{Average}, \qquad (3)$$

where X_{lesion} and $X_{background}$ represent any of the four parameters described in Section II (E) from the lesion and background tissue areas of a patient scan.

III. Results

A. Regularization Coefficient, α

Coefficient α was varied between 2 and 120 for a time series of strain images, and VE parameters were extracted for an infiltrating ductal carcinoma (IDC) lesion. α is proportional to the smoothness of the strain image; Fig. 2a shows the resultant strain images when the coefficient is too small and Fig. 2b shows a normal/smooth strain image. Strain noise suppression increases with α at the cost of spatial resolution. The recommended α value range of 2 to 10 [10] was unable to sufficiently minimize decorrelation noise, so we adopted a value of 40 for processing all patient data.

T_1 values versus α are plotted in Fig. 3 for a malignant lesion. T_1 values are stable for $\alpha > 40$ where much of the strain noise is suppressed. VE lesion contrast calculated in

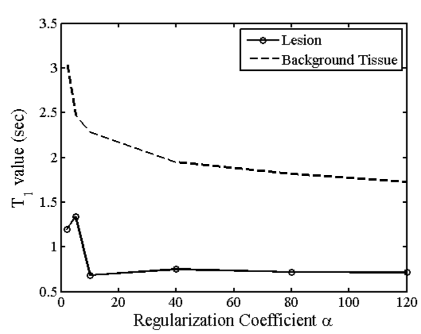

Fig. 3. T_1 estimates from the lesion and background tissues collected at different α values. Values below 40 shows bias in T_1 estimates because of strain noise, as shown in Fig. 2.

this range provided a reliable separation between benign and malignant lesions, thus improving diagnostic performance.

B. Number of scale levels

The default number of scale levels as determined in [10] is I = 5 (6 levels). The anisotropic ratio of 4 is used to account for the ratio of axial-to-lateral block size. The number of scale levels used for our patient data was 6. The effect of the change on the computation time needed to process 166 strain images is shown in Table II. Computational times for 7 scale levels are similar to those for 5 scale levels. However, strain images resulting from 5 scale levels failed to detect small parts of the breast tissue whereas the strain image resulted from 7 scale levels showed additional decorrelation noise. Therefore, the optimal number of scale levels for this study is 6.

TABLE II
T_1 Computation Time for Different Scale Levels

Number of Scale Levels	ROF Computation Time (min)
5	69.2
6	80.8
7	91.3

C. Search Window Size

The default search window size was 8×2 pixels (axial×lateral). For comparison purposes, other search window sizes were used that were determined to be optimal for smaller and larger between-frame compression percentages in [10]. The resultant ROF computation time to process 166 strain images and the resultant T_1 contrast estimates are shown in Table III. Although different search window size yielded similar T_1 contrast values (T_1 = 0.8814 ± 0.0066), the computation time for the strain image sequence increases as the window size increases. A larger window size is ideal when there is a bigger change in the percentage strain between adjacent frames. For this patient study, a search window size of either 4×1 or 8×2 pixels is recommended due to the low percentage of strain between frames.

TABLE III
T_1 Computation Time for Different Search Window Size

Search Window Size	ROF Computation Time (min)	T_1 Contrast
4×1	44.3	-0.8739
8×2	85.8	-0.8865
12×3	157.7	-0.8838

D. Patient data plot

Statistical analysis of image values applied to nonpalbable breast lesions as described in [8] showed little significant contrast in B-mode, ε_0 and ε_1. T_1 was the only discriminating parameter found. VE contrast values are calculated using equation (3) and a scatter plot of elastic strain (ε_0) contrast versus T_1 contrast for each of the 21 patients is shown in Fig.

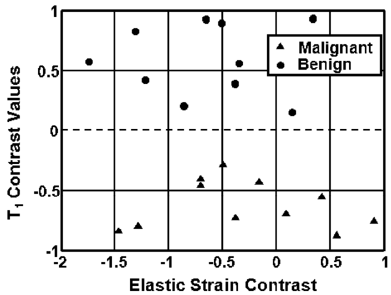

Fig. 4. Scatter plot of patient contrast values for two parameters, ϵ_0 and T_1. A dotted line drawn at T_1 contrast = 0 divides malignant and benign lesions. However, ϵ_0 contrast offers no significant discriminability.

4. In this figure, patients with malignant and benign lesions are clearly separate by the division line at T_1 contrast = 0. T_1 contrast is negative for all malignant lesions and positive for benign lesions studied.

IV. Discussions

In our study, strain images are formed using a regularized multi-scale optical flow algorithm developed by Pellot-Barakat *et al.* [10]. Images of viscoelastic parameters ϵ_0, ϵ_1, and T_1 are produced by curve fitting time-varying strain (creep) curves obtained from fitting strain sequences to an appropriate constitutive model. Parameters used in the formation of the strain images can influence the shape of the curve, and, subsequently, images of the VE parameters.

If a data set is collected properly, then the default options (as mentioned in [10] for breast tissue except for the regularization coefficient) yields a series of strain images that produces relatively smooth creep curves. However, in the case of poor echo data acquisition caused by inappropriate patient or transducer movement, the strain images will contain significant decorrelation noise and the algorithm would be unable to produce a creep curve that follows the model, e.g., Fig. 1. Nevertheless, adjustments can be made to the ROF algorithm parameters that suppress the noise without greatly increasing computational time or degrading spatial resolution.

We are also attempting to adapt the ROF algorithm for the viscoelastic imaging of tissue-mimicking phantoms using the Sonix RP ultrasound system (Ultrasonix Medical Corporation, CA). The advantage of the Sonix RP system is the ability to program most transmit and receive aperture features, as well as the temporal pulse profile. However, the Sonix RP scanner has only half the sampling frequency as the Antares and the linear array pitch is about twice that of the Antares linear array. Since the ratio of axial and lateral sampling is different than that of the Siemens Antares scanner, a new anisotropic block value is needed. The regularization parameter may need to be adjusted to suit the phantom image processing. A good place to start would be testing α values between 2 and 10 to find a balance between strain smoothness and accuracy. The number of scale levels should remain at 6 initially, since this is shown to produce the optimal strain image. If decorrelation noise is significant, the number of scale levels should be lowered. The total percentage strain of the phantom is much higher than that of the breast tissue. Therefore, a larger search window is needed to locate global minimums.

V. Conclusions

Diagnosis of nonpalpable breast lesions can be significantly improved by the inclusion of viscoelastic features information. The ROF strain image processing algorithm must be fine tuned to adapt to the clinical patient scans. It is necessary to find the balance in noise suppression, strain estimation accuracy and computation time in order to achieve the optimal strain images that can be used for VE parameter estimations. The preliminary clinical study has demonstrated the ability of viscoelastic parameters in the characterization and differentiation of nonpalpable breast lesions. The addition of viscoelastic features into the diagnostic feature space can aid physicians in making more accurate and prompt diagnosis of patients with early breast cancer.

Acknowledgment

Special thanks to Mallika Keralapura, Karen Lindfors, Pamela Phelps and Tonya Sheppard.

References

[1] American Cancer Society (2007). Cancer Facts & Figures 2007. Available: http://www.cancer.org/downloads/STT/BCFF-Final.pdf

[2] F. Moinfar, Y. G. Man, L. Arnould, G. L. Bratthauer, M. Ratscheck, F. A. Tavassoli, "Concurrent and independent genetic alterations in the stromal and epithelial cells of mammary carcinoma: implications for tumorigenesis," *Can. Res.,* vol. 60, May 2000, pp.2562-2566.

[3] J. F. Greenleaf, M. Fatemi, M. Insana, "Selected methods for imaging elastic properties of biological tissues," *Annual Review of Biomedical Engineering,* vol. 5, April 2003, pp.57-78.

[4] A. Thomas, S. Kümmel, F. Fritzsche, M. Warm, B. Ebert, B. Hamm, T. Fischer, "Real-time sonoelastography performed in addition to B-mode ultrasound and mammography: improved differentiation of breast lesions," *Acad. Radiol.*, vol. 13, Aug. 2006, pp.1496-1504.

[5] A. Thomas, M. Warm, M. Hoopmann, F. Diekmann, T. Fischer, "Tissue Doppler and strain imaging for evaluating tissue elasticity of breast lesions," *Acad. Radiol.*, vol. 14, May 2007, pp.522-529.

[6] H. Zhi, B. Ou, B. M. Luo, X. Feng, Y. L. Wen, H. Y. Yang, "Comparison of ultrasound elastography, mammography, and sonography in the diagnosis of solid breast lesions," *J. Ultrasound Med.,* vol. 26, Jun 2007, pp.807-815.

[7] M. Sridhar, M. F. Insana, "Ultrasonic measurements of breast viscoelasticity," *Med. Phys.,* vol. 34, Dec. 2007, pp.4757-4767.

[8] Y. Qiu, M. Sridhar, J. K. Tsou, K. K. Lindfors, M. F. Insana, "Ultrasonic viscoelasticity imaging of nonpalpable breast tumors: preliminary results," *Acad. Radiol.*, vol. 15, Dec. 2008, pp.1526–33.

[9] H. Du, J. Liu, C. Barakat, M. F. Insana, "Optimizing multicompression approaches to breast elasticity imaging," *IEEE Trans. Ultrason. Ferroelec. Freq. Control*, vol 53, Jan 2006, pp.90-99.

[10] C. Pellot-Barakat, F. Frouin, M. F. Insana, "Ultrasound elastography based on multiscale estimations of regularized displacement fields," *IEEE Trans. Medical Imaging*, vol. 23, Feb. 2004, pp.153-163.

[11] M. Sridhar, J. Liu, M. F. Insana, "Viscoelasticity imaging using ultrasound: parameters and error analysis," *Phys. Med. Biol.*, vol. 52, May 2007, pp.2425-2443.

[12] C. Pellot-Barakat, F. Frouin, A. Herment, J. J. Mai, K. K. Lindfors, J. K. Tsou, P. Von Behren, M. F. Insana, "A regularized approach for freehand ultrasound elastography of breast lesions," *Biomedical Imaging: Nano to Macro*, IEEE International Symposium on, vol. 1, April 2004, pp. 952-955.